Journal of Pharmaceutical Analysis 13 (2023) 1281–1295

Contents lists available at ScienceDirect

Journal of Pharmaceutical Analysis

journal homepage: www.elsevier.com/locate/jpa

Original article

Oridonin restores hepatic lipid homeostasis in an LXRα-ATGL/EPT1 axis-dependent manner

Yulian Chen [a, 1], Huanguo Jiang [a, 1], Zhikun Zhan [a, 1], Jindi Lu [a], Tanwei Gu [a], Ping Yu [a], Weimin Liang [a], Xi Zhang [a], Shilong Zhong [a, b], Lan Tang [a, *]

[a] NMPA Key Laboratory for Research and Evaluation of Drug Metabolism, Guangdong Provincial Key Laboratory of New Drug Screening, School of Pharmaceutical Sciences, Southern Medical University, Guangzhou, 510515, China
[b] Department of Pharmacy, Guangdong Provincial People's Hospital (Guangdong Academy of Medical Sciences), Southern Medical University, Guangzhou, 510515, China

ARTICLE INFO

Article history:
Received 1 March 2023
Received in revised form
1 August 2023
Accepted 10 August 2023
Available online 21 August 2023

Keywords:
Oridonin
Lipid homeostasis
TG reduction
PE elevation
LXRα-ATGL/EPT1 axis

ABSTRACT

Hepatosteatosis is characterized by abnormal accumulation of triglycerides (TG), leading to prolonged and chronic inflammatory infiltration. To date, there is still a lack of effective and economical therapies for hepatosteatosis. Oridonin (ORI) is a major bioactive component extracted from the traditional Chinese medicinal herb *Rabdosia rubescens*. In this paper, we showed that ORI exerted significant protective effects against hepatic steatosis, inflammation and fibrosis, which was dependent on LXRα signaling. It is reported that LXRα regulated lipid homeostasis between triglyceride (TG) and phosphatidylethanolamine (PE) by promoting *ATGL* and *EPT1* expression. Therefore, we implemented the lipidomic strategy and luciferase reporter assay to verify that ORI contributed to the homeostasis of lipids via the regulation of the *ATGL* gene associated with TG hydrolysis and the *EPT1* gene related to PE synthesis in a LXRα-dependent manner, and the results showed the TG reduction and PE elevation. In detail, hepatic TG overload and lipotoxicity were reversed after ORI treatment by modulating the *ATGL* and *EPT1* genes, respectively. Taken together, the data provide mechanistic insights to explain the bioactivity of ORI in attenuating TG accumulation and cytotoxicity and introduce exciting opportunities for developing novel natural activators of the LXRα-ATGL/EPT1 axis for pharmacologically treating hepatosteatosis and metabolic disorders.

1. Introduction

In modern society, owing to excessive and unbalanced energy intake leading to a drastic increase in obesity, dysregulation of hepatic lipid homeostasis becomes prevalent and gradually develops into hepatosteatosis [1–3]. Hepatosteatosis covers a clinicopathological spectrum of liver disorders with the initial accumulation of ectopic hepatic triglycerides (TGs) progressing to nonalcoholic fatty liver disease (NAFLD), and even nonalcoholic steatohepatitis (NASH), which is characterized by the presence of extensive inflammation in the liver [4,5]. Recent studies indicate that abnormal TG accumulation is usually accompanied by impaired phospholipid homeostasis, which further destroys systemic lipid homeostasis, thereby aggravating the lipotoxicity and liver malfunction [3,6,7]. Since the liver is the nexus for lipid synthesis and metabolism, the repair of hepatic lipid homeostasis by regulating intrinsic mechanisms is a promising treatment for hepatosteatosis and associated metabolic disorders caused by excessive energy intake.

For a healthy lipid cycle in vivo, TG, as the most abundant neutral lipid, is hydrolyzed to diglyceride (DG) by adipose triglyceride lipase (ATGL) [8,9]. On the one hand, DG can be further decomposed into free fatty acids (FFAs) for oxidative metabolism and energy supply. On the other hand, DG is a precursor of phosphatidylethanolamine (PE) in the cytidine diphosphate ethanolamine (CDP-Etn) pathway, a process regarded as the principal route for PE synthesis in most mammalian tissues [10,11]. Phosphoethanolamine (P-Etn) is modified to produce CDP-Etn, which, together with DG, is catalyzed by the ethanolamine phosphotransferase 1 (EPT1) enzyme to generate PE [12,13]. As the second most abundant phospholipid in mammalian membranes, PE plays

Peer review under responsibility of Xi'an Jiaotong University.
* Corresponding author.
E-mail address: tl405@smu.edu.cn (L. Tang).
[1] These authors equally contributed to this work.

https://doi.org/10.1016/j.jpha.2023.08.010

an integral role in membrane architecture and makes up the lipid bilayer of the cell membrane [14]. PE is also involved in anti-inflammatory, proapoptotic, autophagic, and cell membrane fusion functions [15]. While energy oversupply begets disruption of hepatic lipid homeostasis, prolonged inappropriate TG deposition at ectopic hepatocellular sites resulting in breakdown of phospholipid bilayer integrity is referred to as lipotoxicity, ensuing inflammatory response and hepatocyte apoptosis [3,6,9,16].

Liver X receptor (LXR) plays a key role in the regulation of anti-inflammatory and lipid homeostasis [17–19]. Our previous study revealed that LXRα regulated lipid homeostasis between TG and PE to alleviate hepatosteatosis by boosting *ATGL* and *EPT1* expression [20]. Clearly, a growing body of evidence is revealing the significance of homeostasis between TG and PE in hepatic steatosis [21], which supports the rationale of activating the hepatic LXRα-ATGL/EPT1 pathway for treating obesity-associated hepatosteatosis.

Oridonin (ORI), a bioactive ent-kaurane diterpenoid, mainly exists in Chinese herb *Rabdosia rubescens* with potent pharmacological activities including anti-inflammatory, antitumor and antibacterial effects [22–24]. Currently, *R. rubescens* is a commonly available Chinese over-the-counter (OTC) herbal medicine for the treatment of inflammatory diseases [25,26]. Besides, limited research has suggested that ORI may contribute to improving the pathophysiology of NAFLD by exerting anti-inflammatory effects via the NLR family pyrin domain containing 3 (NLRP3) interaction or ROS-NF-κB suppression [27,28]. Our previous study also reported that ORI ameliorated acute liver injury-induced liver inflammation by inhibiting the NLRP3 inflammasome [29]. However, the function of ORI restoring lipid homeostasis to ameliorate hepatosteatosis and NAFLD, especially its exact molecular mechanism, has not been explored.

Due to its low cost, effectiveness, and few side effects, the role of using traditional Chinese medicine in handling chronic metabolic diseases such as obesity and NAFLD has been recognized by the public at large [30]. Nevertheless, its complex composition and unclear pharmacology limit its clinical application. Our work showed that ORI induced LXRα expression, which is essential for lipid homeostasis between TG and PE, and subsequently exerted its anti-steatosis and hepatoprotective activity. Our findings not only provide the first line of evidence that ORI ameliorates hepatosteatosis by preserving lipid homeostasis between TG and PE in an LXRα-ATGL/EPT1 axis-dependent manner, but also open exciting opportunities for developing ORI as a promising drug candidate for hepatosteatosis.

2. Materials and methods

2.1. Materials

ORI was obtained from Chengdu Alfa Biotechnology Co., Ltd. (Chengdu, China). The liver X receptor agonist GW3965 (405911-17-3) was purchased from Selleck (Shanghai, China). The primary antibodies for Western blotting were as follows: anti-LXRα antibody (1:500 dilution, ab41902, ab176323, Abcam, Cambridge, UK), anti-EPT1 antibody (1:250 dilution, ab194554, Abcam), anti-ATGL antibody (1:500 dilution, DF7756, Affinity, Liyang, China), anti-GAPDH antibody (1:3000 dilution, ab8345, Abcam), HRP-conjugated goat anti-rabbit IgG (1:3000 dilution, ab6721, Abcam), HRP-conjugated goat anti-mouse IgG (1:3000 dilution, ab6789, Abcam). Cy7-labeled cholesterol and cy7-labeled phosphoethanolamine were purchased from Xi'an Qiyue Biotechnology Co., Ltd (Xi'an, China). The small interfering RNA (siRNA) specific for LXRα (sc-38828), ATGL (sc-60223) and EPT1 (sc-61516), and negative control siRNA (sc-37007) were obtained from Santa Cruz Biotechnology (Dallas, TX, USA). LXRα plasmids (EX-A1306-M02) were purchased from GeneCopoeia Inc. (Guangzhou, China). ATGL and EPT1 luciferase reports and pRL-nTK were obtained from Transheep (Shanghai, China). Lipofectamine™ 3000 Transfection Reagent (L3000001) was purchased from Invitrogen Life Technologies (Carlsbad, CA, USA). HepG2 cells were purchased from ATCC (Philadelphia, PA, USA). Triglyceride (TG) (A110-1-1) assay kit was obtained from Jiancheng Bioengineering Institute (Nanjing, China). Tumor necrosis factor (TNF-α) (A104732) and interleukin 1 beta (IL-1β) (A105903) ELISA kits for mouse liver tissue were obtained from Shanghai Fusheng Industrial Co. (Shanghai, China).

2.2. Animal models

Wild-type (WT) C57BL/6 mice were obtained from the laboratory animal center of Southern Medical University (Guangzhou, China). LXRα$^{-/-}$ knockout mice (KOCMP-21253-Nr1h3) have been produced and verified by Cyagen Biosciences (Guangzhou) Inc. (Guangzhou, China). Genotyping of mice was performed with primers F1: 5′-CTGCAACCAACACCAGTCTTCAATC-3′, R1: 5′-CTAAAGCAAGAATGAAGGCCACTGC-3′ and F2: 5′-CTCTGCAATC-GAGGTGGCTGGAAAG-3′. All mice were housed in pathogen-free conditions with free access to water and chow in a 12/12 h light/dark cycle. Animals used were permitted by the Institutional Animal Care and Use Committee of Southern Medical University (Approval number: SMUL2020155).

2.3. Mouse high-fat diet (HFD) model and ORI treatment

Male mice (6–8 weeks old) were fed with chow diet (SPF-F02-002, SPF (Beijing) Biotechnology Co., Ltd., Beijing, China) or HFD (60% calories from fat, HF60, Dyets, Inc., Bethlehem, PA, USA) for 24 weeks. In addition, mice were treated with ORI (50 mg/kg or 100 mg/kg), atorvastatin (10 mg/kg) or vehicle (5% Tween 80, 20% PEG400, 5% HPMC) by oral gavage once a day from 16th to 24th week. The mice were sacrificed by exsanguination under anesthesia with inhaled 5% isoflurane. Blood samples, adipose and liver tissues were collected for further analysis.

2.4. Biochemical analyses

Pointcare automatic biochemical analysis system (S/N:31919, MNCHIP, Tianjin, China) was used to detect serum triglyceride (TG), total cholesterol (CHOL), alanine aminotransferase (ALT) and aspartate aminotransferase (AST) levels according to the manufacturer's instructions.

Glucose tolerance test (GTT) and insulin tolerance test (ITT) were monitered in mice fasted for 12 and 6 h, respectively. For GTT, mice were intraperitoneally injected with 1 g/kg glucose, while 0.75 IU/kg insulin was intraperitoneally injected into mice for ITT. Blood glucose was tested before (time 0) and at 15, 30, 60 and 120 min after injection by Handheld blood glucose meter.

Mice fasted for 12 h were gavaged with olive oil (10 μL/g). Blood sample was collected by orbital bleeding before (time 0) and at 15, 30, 60, 120, and 240 min after oil gavage for TG measurement with assay kit (A110-1-1, Nanjing Jiancheng Bioengineering Institute, Nanjing, China). After 2 h post gavage, the plasma and liver samples were collected and imaged to detect lipid accumulation. The area under the curve (AUC) was calculated by Prism 7 software (GraphPad).

2.5. Lipidomic profiling

Lipid metabolite profiling was performed using a targeted quantitative lipidomics by Wuhan Metware Biotechnology Co., Ltd. (Wuhan, China). Frozen liver tissue (50 mg) was homogenized in

1 mL lipid extract (methyl tert-butyl ether:methanol = 3:1). Tissue samples were whirled the mixture at 4 °C for 2 min. Then, 200 μL of deionized H_2O was added to the mixture, followed by centrifuged at 16,000 × *g* at 4 °C for 10 min. The extract supernatant was dried and redissolved. Then, a liquid chromatography-electrospray ionization-tandem mass (LC-ESI-MS/MS) system (UHPLC, ExionLC™AD, Framingham, MA, USA; MS, QTRAP® 6500+, Framingham) was performed for metabolite quantification. The internal standards are shown in Table S1. Overall, the analytical conditions of UHPLC were as follows: solvent system: A: acetonitrile/water (60/40, *V/V*) containing 0.1% methanoic acid and 10 mmol/L ammonium formate; B: acetonitrile/isopropanol (10/90, *V/V*) containing 0.1% methanoic acid and 10 mmol/L ammonium formate; a graded series of A/B programme: 80:20 (*V/V*) at 0 min, 70:30 (*V/V*) at 3.0 min, 40:60 (*V/V*) at 4 min, 15:85 (*V/V*) at 9 min, 10:90 (*V/V*) at 14 min, 5:95 (*V/V*) at 15.5 min, 5:95 (*V/V*) at 17.3 min, 80:20 (*V/V*) at 17.5 min and 80:20 (*V/V*) at 20 min; column: Thermo C30 (2.1 mm × 100 mm, 2.6 μm, MA, USA); flow rate: 0.35 mL/min; temperature: 45 °C; injection volume: 2 μL. After quality control, a total of 473 lipid metabolites were detected.

2.6. Transcriptome

Total RNA isolation was performed using the RNAprep Kit (RE-03014, FOREGENE, Chengdu, China) according to the manufacturer's instructions. Transcriptome libraries were produced and sequenced on the Illumina HiSeq 4000 using 150 bp paired-end reads (Novogene, Beijing, China). The low-quality reads were filtered out following the quality control procedures and used for the genome assembly. The gene expression levels were assessed as the number of reads per kilobase of gene length per million mapped reads (FPKM). RNA-seq data were obtained from GEO database with an accession number of GSE112908.

2.7. Bioluminescence imaging

Cy7-labled phosphoethanolamine (6.25 mg/kg) or cy7-labeled cholesterol (10 mg/kg) was injected into tail vein of isoflurane anesthetized animals, and then the in vivo bioluminescence imaging was performed. Images were detected using a multimodal small-animal in vivo imaging system (FX Pro, Bruker, Karlsruhe, Germany) with an open filter.

2.8. Human sample collection

Human liver tissues were obtained from Sun Yat-Sen Memorial Hospital (Guangzhou, China). Healthy tissues surrounding the primary tumor (Normal) or nonalcoholic fatty liver (NAFL) were isolated, and only histologically non-tumorous tissues were used. All tissue samples were stored in liquid nitrogen for later experiments. Approvals were obtained from the ethics committee of Sun Yat-Sen Memorial Hospital (Approval number: ECSYS NO. CS07095).

2.9. Histological analysis

The liver and adipose tissue was fixed in 4% paraformaldehyde solution (Solarbio, Beijing, China), dehydrated, and embedded in paraffin. Histology was performed on 6–10 μm paraffin-embedded sections by staining them with hematoxylin & eosin (H&E) and Masson's trichrome.

In the view of oil red O (ORO) staining, liver samples were frozen at −80 °C and embedded in optimal cutting temperature (OCT) compound. 10 μm thick sections were prepared and stained with ORO.

Hematoxylin counterstaining was performed after the above staining. Images were captured using CX-31 microscope (Olympus, Tokyo, Japan). The adipocyte size (iWAT and iBAT) was measured using the ruler tool in the NanoZoomer Digital Pathology software (HAMAMATSU, Hamamatsu, Japan). And the stained area of the lesion was determined by ImageJ software based on six sections per mouse and six mice per group.

For immunofluorescence staining of LXRα, ATGL and EPT1 in liver sections, the sections were blocked with 5% bovine serum albumin (BSA), followed by incubation with primary antibodies (dilution ratio, 1:100, *V/V*) at 4 °C overnight. After a three-time wash with Tris Buffered Saline Tween (TBST), sections were incubated with second antibody for 1 h. After TBST was removed, the sections were incubated in 4,6-diamino-2-phenyl indole (DAPI) in the dark for 5 min to stain nuclei. Immunofluorescence images were obtained with the Olympus BX-53 microscope (Olympus, Tokyo, Japan).

2.10. Molecular assays

To determine mRNA levels, total RNA was isolated using RNAprep Kit (RE-03014, FOREGENE, Chengdu, China) and reversely transcribed to cDNA using RT Master Mix (RR037A, Takara, Shiga, Japan). SYBR Green Master Mix (A6002, Promega, Madison, WI, USA) was used for carrying out qPCR. Data were normalized to the housekeeping gene (*GAPDH*). Primers are listed in Table S2.

Protein extracts (25 μg) were separated by 10% sodium dodecyl sulfate-polyacrylamide gel electrophoresis (SDS-PAGE) and then transferred to polyvinylidene fluoride membranes (Millipore, Darmstadt, Germany) for 1.5 h by wet transfer method. After being blocked with 5% skimmed milk, the membranes were incubated with primary antibody overnight at 4 °C, followed by crosslinking with HRP-conjugated secondary antibody. Protein bands were visualized by using FluorChem R system (ProteinSimple, San Francisco, CA, USA). The band densities of each stripe was calculated by ImageJ software.

2.11. Cell culture

HepG2 and 293T cell line were purchased from American Tissue Culture Collection (Manassas, VA, USA). Cells cultured in Dulbecco's modified Eagle's medium (DMEM) (10270106, Gibico, New York, NY, USA) supplemented with 10% fetal bovine serum (FBS) (FSP500, ExCell Bio, Taicang, China) at 37 °C under 5% CO_2. Cells were transfected with siRN ExCell Bio A using Lipofectamine™ 3000 Transfection Reagent (L3000001, Invitrogen Life Technologies).

10 mM ORI as a mother solution was dissolved using dimethyl sulfoxide (DMSO) and subsequently diluted to 5 μM or 10 μM with cell-culture medium. The control group was treated with medium containing 1‰ DMSO.

For the establishment of NAFLD model in vitro, HepG2 cells were administrated with cell culture medium containing the indicated concentrations of palmitic acid (PA) (0.25 mM) and oleic acid (OA) (0.5 mM) (SYSJ-KJ006, Kunchuang, Xi'an, China) for 48 h.

2.12. Luciferase assay

Before transfection, HepG2 and 293T cells were grown to 70%–90% confluence in 24-well plates. Cells were co-transfected with ATGL or EPT1 luciferase reporter (300 ng), pRL-nTK (a renilla luciferase reporter, 60 ng) and overexpression LXRα plasmid (600 ng) by incubation with Lipofectamine™ 3000 Transfection Reagent. On the next day, cells were treated with 10 μM ORI or 10 μM GW3965 solvent control for another 24 h in complete medium. Luciferase activities were measured with the Luciferase Assay System (E1910, Promega, Madison, WI, USA).

2.13. Cell Counting Kit-8 (CCK8)

The working solution was prepared using CCK8 reagent (CK04, Dojindo, Kyushu Island, Japan) mixed with DMEM (1:10, *V*/*V*). Next, the supernatant was removed from the cells in 96-well plate and 110 μL of working solution was added to incubate at 37 °C for 1 h. Absorbance was measured at 450 nm to assess cell viability.

2.14. Nile red (NR) fluorescence determination and staining with DAPI

NR powder (7385-67-3, Biotopped, Beijing, China) was formulated into a 1 mg/mL stock solution with DMSO. Stock solution was diluted by PBS at a dilution of 1:2000 (*V*/*V*) to prepare a working solution. Each well of the 96-well plate was incubated with 100 μL working solution for 15 min, and washed three times with PBS. After setting the excitation light wavelength of the microplate reader (M1000PRO, TECAN, Männedorf, Switzerland) to 485 nm and the emission wavelength to 580 nm, the fluorescence intensity was determined.

In the case of the NR staining, cells were incubated in 4% paraformaldehyde for 30 min. NR staining was carried out as described above. Later, the cell samples were covered in the DAPI (C0065, Solarbio) solution for 5 min. The images were detected by Inverted Fluorescence Microscope (Axio Observer A1, Carl Zeiss, Oberkochen, Germany).

2.15. Hepatic TG and CHOL determination

Samples of animal liver tissue and cells were sonicated in ethanol to determine TG and CHOL levels using assay kit (A110-1-1 and A111-1-1, Jiancheng Bioengineering Institute, Nanjing, China). Then, protein concentration was determined using the BCA method (P0012, Beyotime, Shanghai, China). TG and CHOL content wwere normalized by protein concentration.

2.16. Statistical analysis

All experiments, except the in vivo mouse studies, were performed at least three times. All data are expressed as mean ± standard deviation (SD). Statistical analysis was performed using Prism 7 software (GraphPad). Groups were compared by unpaired two-tailed Student's t-test or two-way analysis of variance (ANOVA) followed by post-hoc Bonferroni test. $P < 0.05$ was considered to be significant ($^{*}P < 0.05$, $^{**}P < 0.01$).

3. Results

3.1. ORI attenuates HFD-induced hepatic steatosis and inflammation

Mice were fed a HFD for 16 weeks and then administered with ORI (ORI) (50 and 100 mg/kg) and atorvastatin (10 mg/kg) while continuing to receive the HFD for an additional 8 weeks ($n = 6$) (Fig. S1A). There was a remarkable increase of lipid accumulation and body weight in HFD-fed mice compared with chow-fed mice (Figs. 1A and B). In the morphologic photographs, ORI administration showed less lipid deposition and a more normal liver morphology (Fig. 1A). When the food intake was not altered by ORI treatment (Fig. S1B), the body weight of mice treated with ORI was significantly inhibited (Fig. 1B). After 24 weeks of HFD feeding, the liver weights and liver weight-to-body weight ratios of the HFD-fed mice were significantly increased. In contrast, the liver weights and liver weight-to-body weight ratios were significantly decreased in mice treated with ORI (Figs. 1C and D). Compared with HFD mice, ORI-treated mice exhibited significantly lower hepatic and plasma TG and CHOL levels (Figs. 1E and F). In histological analysis of liver sections, it was showed that mice treated with ORI exhibited less hepatocyte injury (ballooning), lobular inflammation, steatosis and hepatic fibrosis as compared to mice fed with HFD (Figs. 1G and H). HFD induced blood activities of ALT and AST, which were partly suppressed by ORI (Fig. 1I). Consistently, the hepatic levels of IL-1β and TNF-α were lower in ORI-treated mice (Figs. 1J and K).

In addition, ORI treatment prevented the weight of inguinal white adipose tissue (iWAT) and interscapular brown adipose tissue (iBAT) (Figs. 2A and B). Histological analysis exhibited that dramatically adipocyte hypertrophy was significantly decreased by ORI (Figs. 2C and D). Besides, HFD-fed mice impaired glucose tolerance as well as insulin sensitivity, which were alleviated by ORI (Figs. 2E–J). Atorvastatin is a clinically effective drug for hyperlipidemia. In our study, atorvastatin treatment showed significant lipid-lowering effect (Figs. 1A–F and 2). However, ORI treatment displayed less hepatic fibrosis and lower levels of inflammatory factors (IL-1β and TNF-α) compared to the atorvastatin treatment (Figs. 1G, H, J and K). Collectively, these results suggest that ORI treatment protect mice against hepatic lipid dysfunction and inflammation induced by HFD feeding.

3.2. LXRα is required for ORI's ability to inhibit the HFD-induced body weight gain and liver injury

In our previous study, we had verified ORI as an effective LXRα inducer [31]. To further confirm the critical role of LXRα in the anti-hepatosteatosis action of ORI, we evaluated whether deletion of LXRα could affect the therapeutic action of ORI (100 mg/kg) in HFD mouse model ($n = 6$) (Fig. S2A). As shown in the morphologic photographs, ORI reduced HFD-induced lipid accumulation in WT mice but this therapeutic effect disappeared in LXRα$^{-/-}$ mice (Fig. 3A). Although ORI treatment and LXRα deletion did not alter food intake, ORI significantly decreased the body weights of WT mice but failed to decrease the body weights of LXRα$^{-/-}$ mice (Figs. S2B and 3B). ORI suppressed the HFD-induced upregulation of liver weight, hepatic and plasma lipid (TG and CHOL) levels in WT mice but not in LXRα$^{-/-}$ mice (Fig. 3C–G). Furthermore, ORI failed to reduce the HFD-induced hepatic steatosis, liver fibrosis, plasma ALT and AST levels in LXRα$^{-/-}$ mice (Figs. 3H–K). ORI also had no effect on the high levels of inflammatory factors (IL-1β and TNF-α) in LXRα$^{-/-}$ mice (Figs. 3L and M).

3.3. LXRα deletion abrogated the improvement of lipid accumulation and insulin resistance in ORI treatment

The reduction in lipid weights (iWAT and iBAT) observed in ORI-treated WT mice was abolished in LXRα$^{-/-}$ mice ($n = 6$) (Figs. 4A and B). The inhibitory action of ORI on HFD-induced adipocyte hypertrophy was abolished in LXRα$^{-/-}$ mice (Figs. 4C and D). Additionally, GTT and ITT demonstrated that deficiency of LXRα was sufficient to abrogate enhancement by ORI of glucose homeostasis (Figs. 4E–H). In line with this, when fasted mice were gavaged olive oil, the HFD-induced hepatic lipid deposition and high circulating TG with increased serum lactescence were ameliorated by ORI in WT mice but not in LXRα$^{-/-}$ mice (Figs. 4I–L). These findings indicate that protection of ORI against hepatic steatosis, inflammation and fibrosis is compromised in LXRα$^{-/-}$ mice.

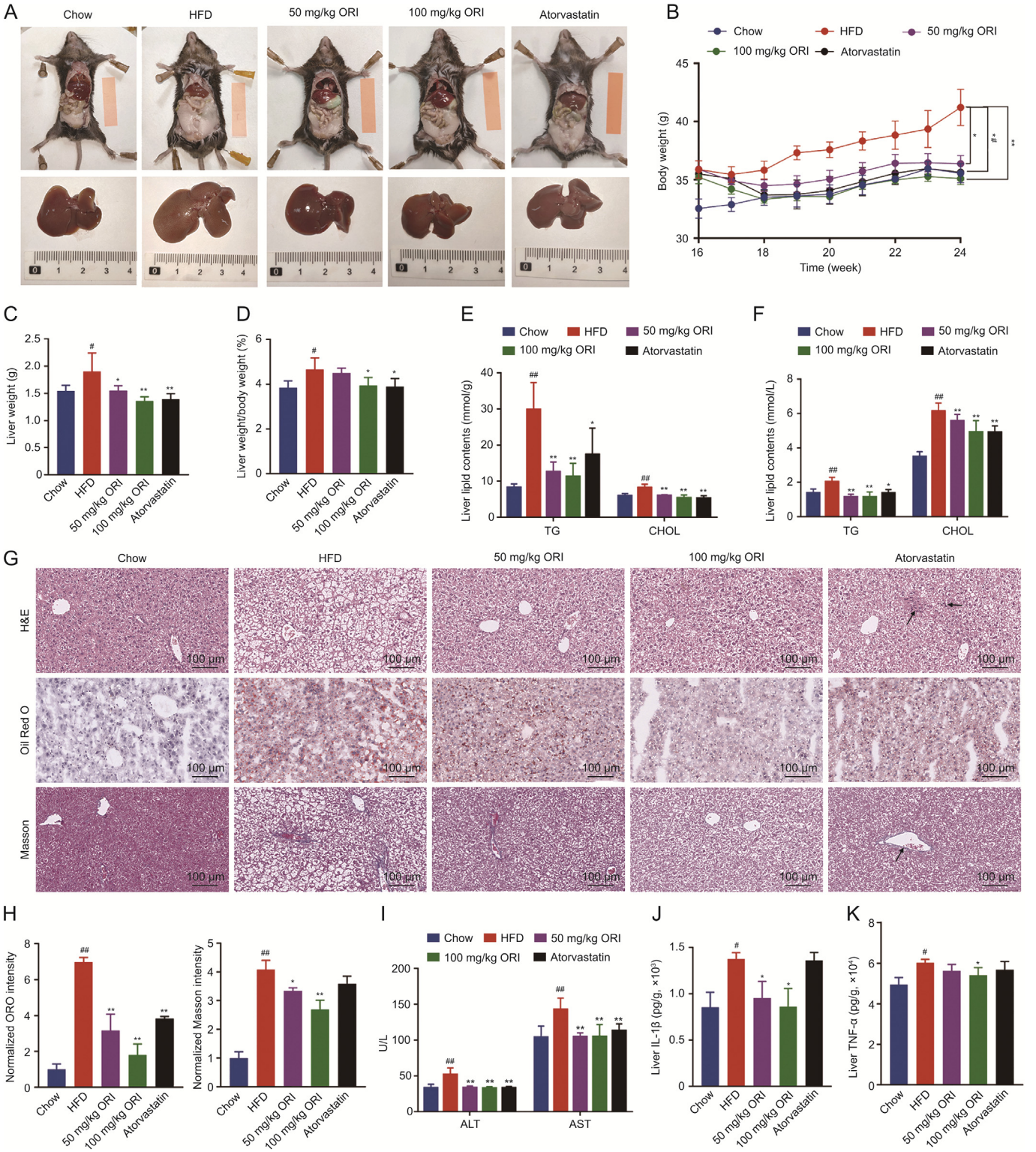

Fig. 1. Oridonin (ORI) attenuates high-fat diet (HFD)-induced body weight gain and liver injury. Except for the control mice, which were fed a normal chow, the other mice were fed a HFD for 24 weeks. Then, mice were randomly assigned to 5 groups: Chow, HFD, 50 mg/kg ORI, 100 mg/kg ORI and Atorvastatin. And the corresponding drug was administrated for the 16–24 weeks in the following assays: (A) Representative liver and adipose tissue photos. (B) Body weight ($n = 6$). (C) Liver weight and (D) liver weight-to-body weight ratios ($n = 6$). (E) Hepatic triglyceride (TG) and cholesterol (CHOL) levels ($n = 6$). (F) Plasma TG and CHOL levels ($n = 6$). (G) Representative hematoxylin & eosin (H&E), oil red O (ORO) and Masson's trichrome staining of liver sections. Black arrows indicate inflammatory cell infiltration and fibrotic lesions. (H) Histological quantification of ORO and Masson's trichrome staining ($n = 6$). (I) Plasma alanine aminotransferase (ALT) and aspartate aminotransferase (AST) levels ($n = 6$). (J) Interleukin 1 beta (IL-1β) and (K) tumor necrosis factor (TNF-α) production (measured by (enzyme-linked immunosorbent assay (ELISA)) in the livers. Data are presented as mean ± standard deviation (SD). $^{\#}P < 0.05$ and $^{\#\#}P < 0.01$ were compared with Chow group; $^{*}P < 0.05$ and $^{**}P < 0.01$ were compared with HFD group.

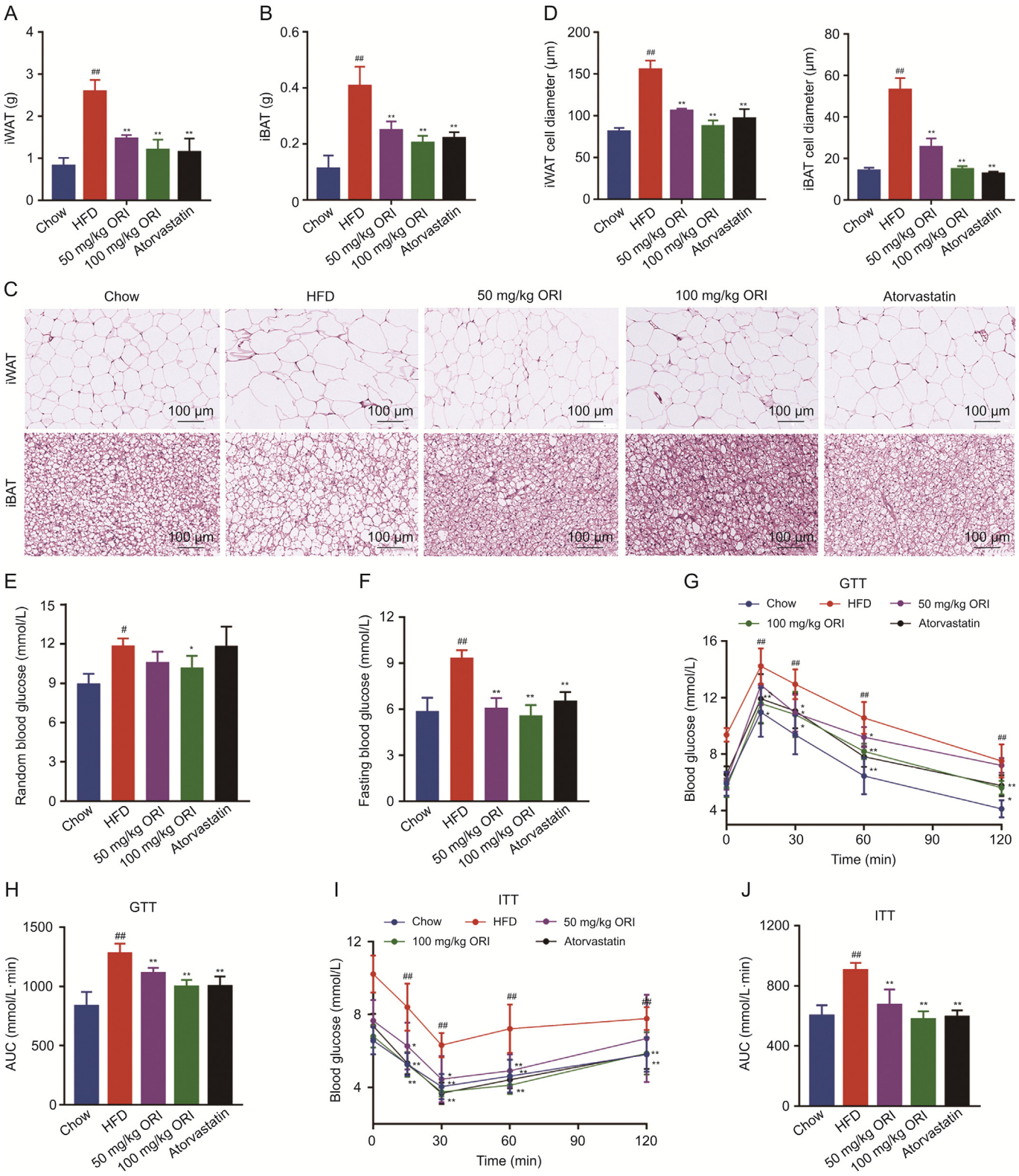

Fig. 2. Oridonin (ORI) alleviates high-fat diet (HFD)-induced obesity and insulin resistance. (A–D) Adipose tissue depots inguinal white adipose tissue (iWAT) and interscapular brown adipose tissue (iBAT) were analyzed for weight (A, B) and adipocyte size (C, D) in the group of Chow, HFD, 50 and 100 mg/kg ORI treatment and atorvastatin treatment ($n = 6$). (E) Random and (F) fasting blood glucose were determined ($n = 6$). (G–J) Glucose tolerance test (GTT) and insulin tolerance test (ITT) were performed ($n = 6$). AUC: area under the curve. Data are presented as mean ± standard deviation (SD). $^{\#}P < 0.05$ and $^{\#\#}P < 0.01$ were compared with Chow group; $^{*}P < 0.05$ and $^{**}P < 0.01$ were compared with HFD group.

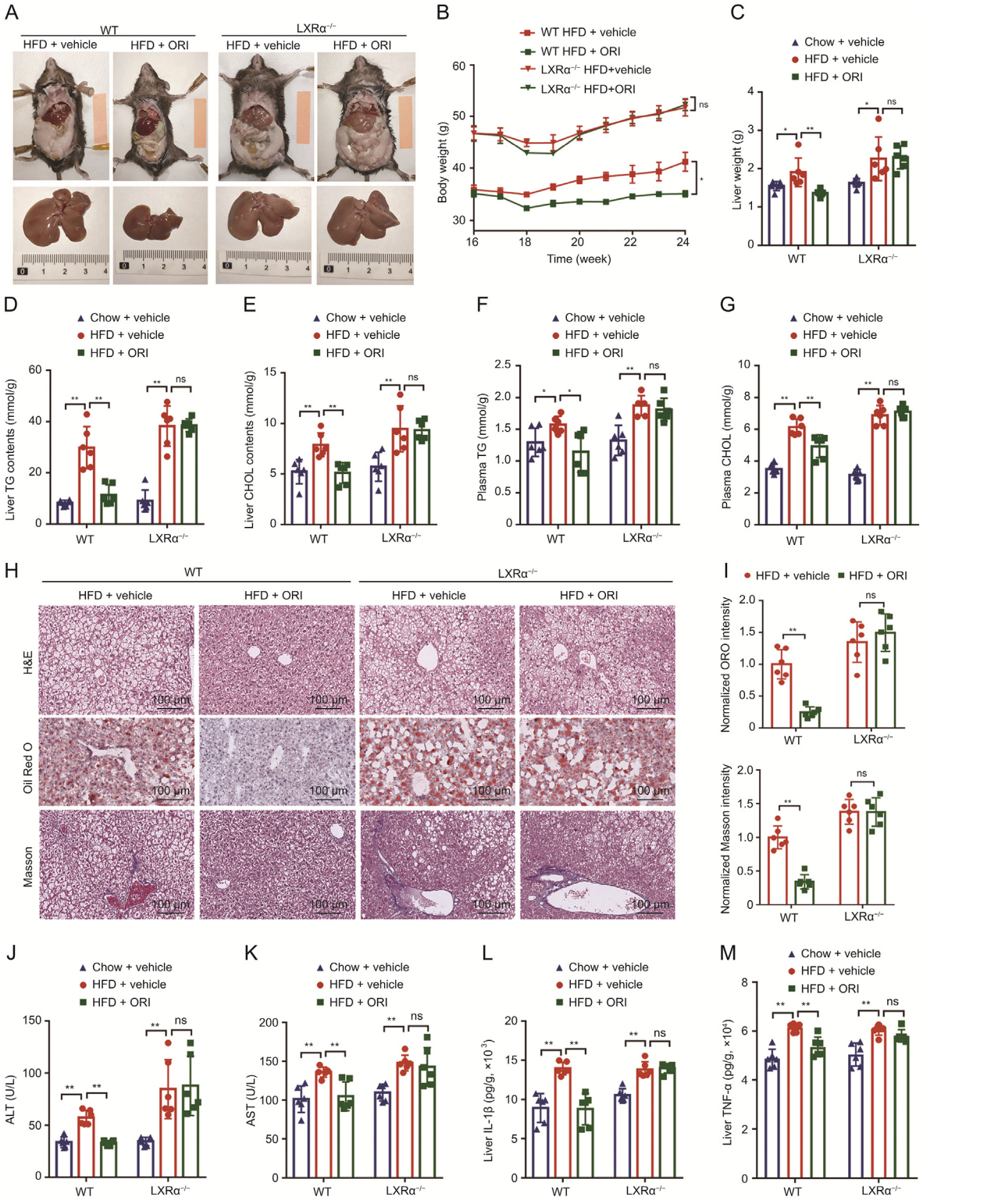

Fig. 3. LXRα is required for oridonin (ORI)'s ability to inhibit the high-fat diet (HFD)-induced body weight gain and liver injury. (A) Representative liver and adipose tissue photos of LXRα$^{-/-}$ mice and wild-type (WT) mice fed on HFD + vehicle or HFD + ORI treatment for the 16–24 weeks. (B) Body weight curves of LXRα$^{-/-}$ mice and WT mice fed on HFD + vehicle or HFD + ORI treatment for the 16–24 weeks ($n = 6$). (C) Liver weight of LXRα$^{-/-}$ mice and WT mice fed on chow, HFD + vehicle or HFD + ORI treatment for the 16–24 weeks ($n = 6$). (D–G) Hepatic triglyceride (TG) (D) and cholesterol (CHOL) (E) levels, and plasma TG (F) and CHOL (G) levels of LXRα$^{-/-}$ mice and WT mice fed on chow, HFD + vehicle or HFD + ORI treatment for the 16–24 weeks ($n = 6$). (H) Representative hematoxylin & eosin (H&E), oil red O (ORO) and Masson's trichrome staining of liver sections from LXRα$^{-/-}$ mice and WT mice fed on chow, HFD + vehicle or HFD + ORI treatment for the 16–24 weeks ($n = 6$). (I) Histological quantification of ORO and Masson's trichrome staining (n = 6). (J) Plasma alanine aminotransferase (ALT) and (K) aspartate aminotransferase (AST) levels of LXRα$^{-/-}$ mice and WT mice fed on chow, HFD + vehicle or HFD + ORI treatment for the 16–24 weeks ($n = 6$). (L) interleukin 1 beta (IL-1β) and (M) tumor necrosis factor (TNF-α) production (measured by ELISA) in the livers from LXRα$^{-/-}$ mice and WT mice fed on chow, HFD + vehicle or HFD + ORI treatment for the 16–24 weeks ($n = 6$). Data are presented as mean ± standard deviation (SD). $^{*}P < 0.05$, $^{**}P < 0.01$, ns: no significance.

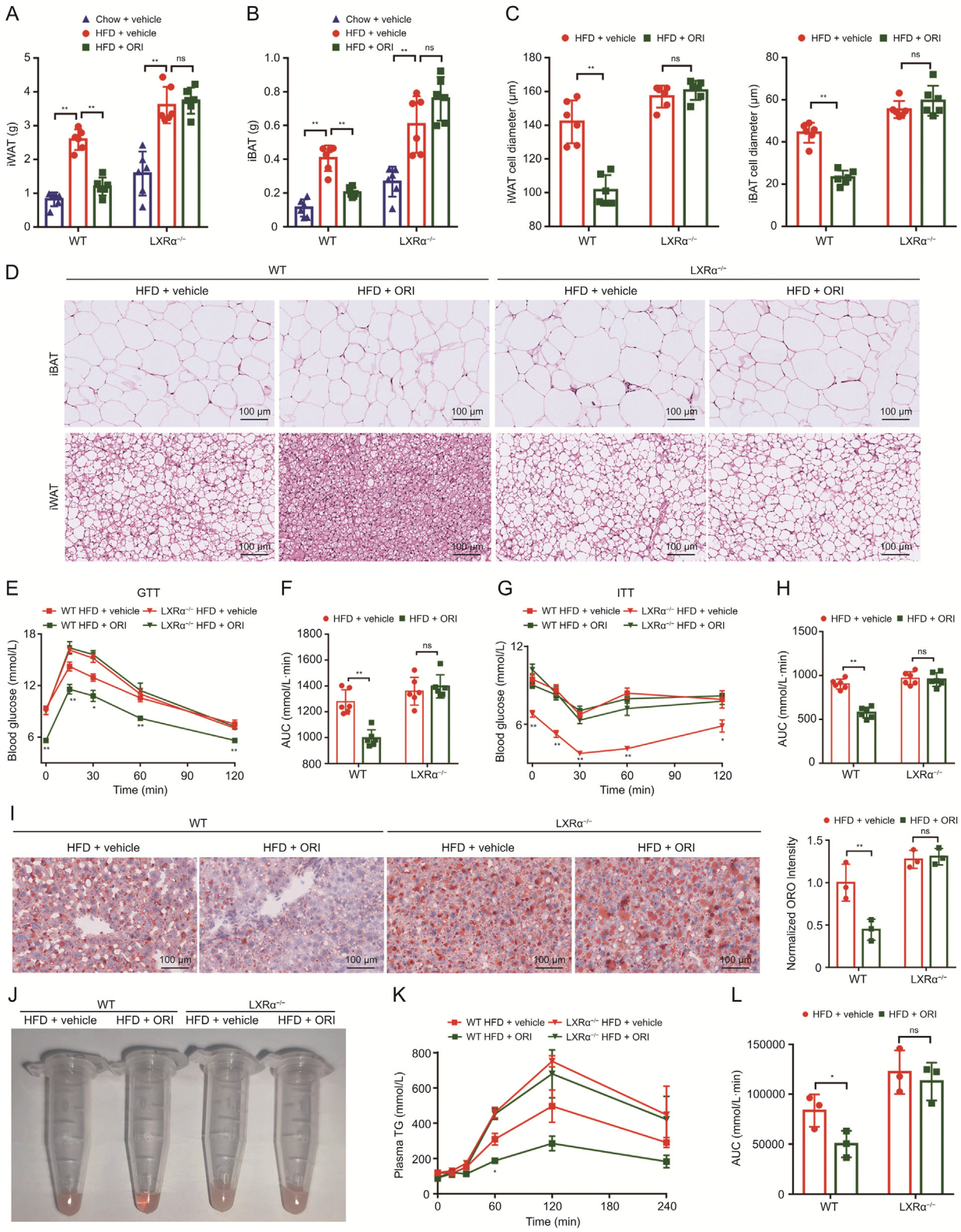

Fig. 4. LXRα deletion abrogated the improvement of lipid accumulation and insulin resistance in oridonin (ORI) treatment. (A–D) The adipose tissue depots inguinal white adipose tissue (iWAT) (A) and interscapular brown adipose tissue (iBAT) (B) of LXRα$^{-/-}$ mice and WT mice, which were fed on chow, high-fat diet (HFD) + vehicle or HFD + ORI treatment for the 16–24 weeks, were determined for weight and adipocyte size (C, D) ($n = 6$). (E–H) Glucose tolerance test (GTT) and insulin tolerance test (ITT) were performed in the LXRα$^{-/-}$ mice and WT mice fed on HFD + vehicle or HFD + ORI treatment for the 16–24 weeks ($n = 3$). (I, J) Image of oil red O (ORO) staining of mouse liver sections (I) and plasma samples (J). Samples were derived from LXRα$^{-/-}$mice and WT mice after oral gavage of olive oil (10μL/g) ($n = 3$). (K) Plasma triglyceride (TG) levels in LXRα$^{-/-}$ mice and WT mice after oral gavage of olive oil (10μL/g) ($n = 3$). (L) The AUC were showed for plasma TG ($n = 3$). Data are presented as mean ± standard deviation (SD). $^{*}P < 0.05$, $^{**}P < 0.01$, ns: no significance.

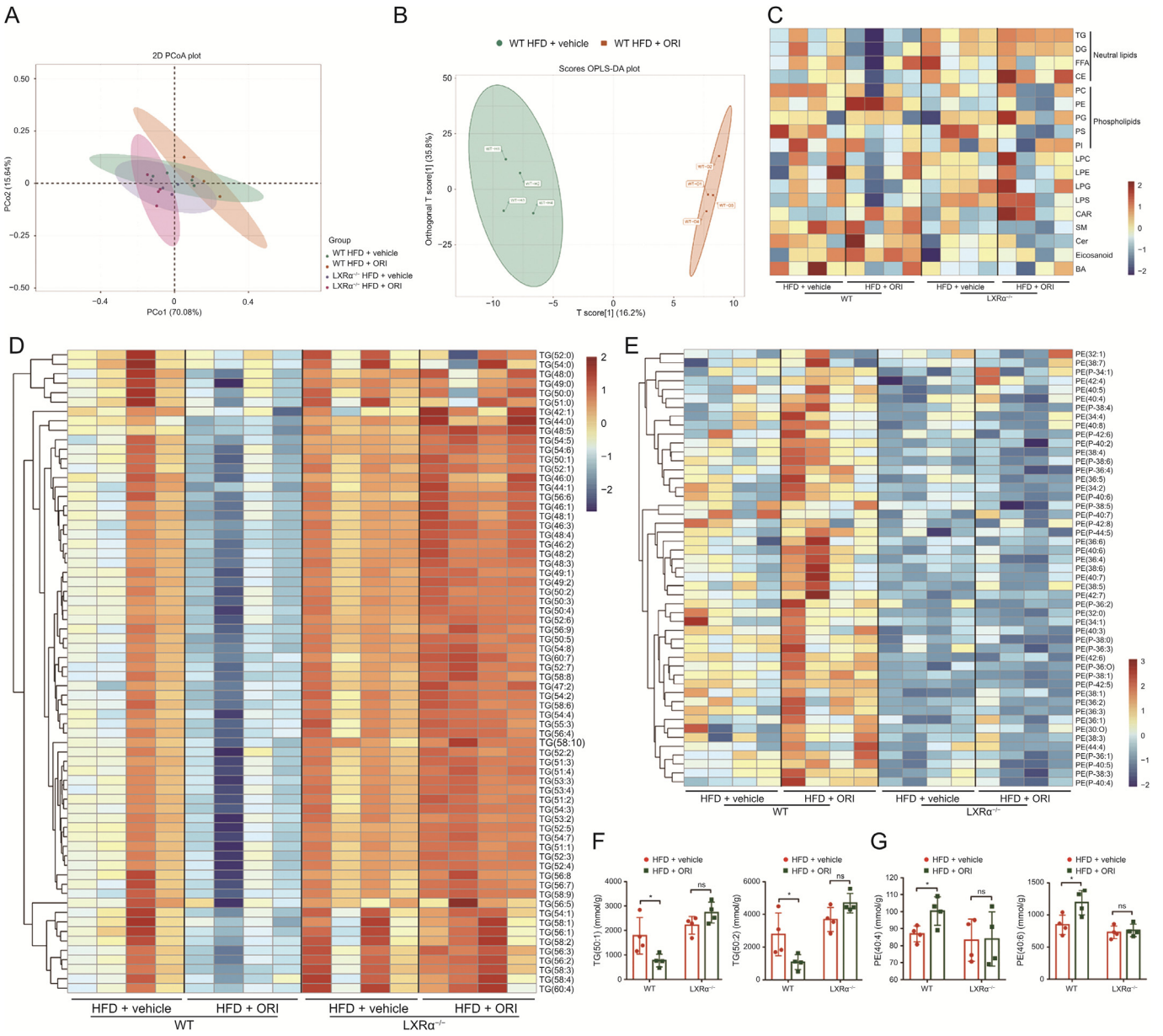

Fig. 5. Lipidomic analysis from the wild-type (WT) or LXR$\alpha^{-/-}$mice induced by a high-fat diet (HFD) with or without oridonin (ORI) treatment. (A) Principal component analysis (PCA) score plot of WT and LXR$\alpha^{-/-}$ mice induced a HFD with or without ORI treatment. (B) Orthogonal partial least squares discrimination analysis (OPLS-DA) score map for WT and LXR$\alpha^{-/-}$ mice fed on a HFD with or without ORI treatment. (C) Heatmap of lipid specie concentrations (nmol/g) in liver tissues from WT and LXR$\alpha^{-/-}$ mice induced a HFD with or without ORI treatment ($n = 4$). (D) Heatmap of species of triglyceride (TG) containing different lengths of fatty acids based on the concentrations (nmol/g) in liver tissues from WT and LXR$\alpha^{-/-}$ mice induced a HFD with or without ORI treatment ($n = 4$). The increased TG species code the color as the red in the heatmap; the decreased ones code the blue. (E) Heatmap of species of phosphatidylethanolamine (PE) containing different lengths of fatty acids based on the concentrations (nmol/g) in liver tissues from WT and LXR$\alpha^{-/-}$ mice induced a HFD with or without ORI treatment ($n = 4$). The increased PE species code the color as the red in the heatmap; the decreased ones code the blue. (F) Abundant and representative concentration (nmol/g) of TG containing different lengths of fatty acids in the liver tissues ($n = 4$). (G) Abundant and representative concentration (nmol/g) of PE containing different lengths of fatty acids in the liver tissues ($n = 4$). Data are presented as mean ± standard deviation (SD). $^{*}P < 0.05$, $^{**}P < 0.01$, ns: no significance.

3.4. ORI restored lipid homeostasis between TG and PE in a LXRα-dependent manner

To investigate the effect and mechanism of ORI on lipid homeostasis, the lipidomics was performed on liver of WT or LXR$\alpha^{-/-}$ mice induced by a HFD with or without ORI treatment. Principal component analysis (PCA) and orthogonal partial least squares discrimination analysis (OPLS-DA) models were carried out to indicate that the lipidomic data of WT mice with ORI treatment clearly separated from those without ORI treatment, which wasn't observed in LXR$\alpha^{-/-}$ mice ($n = 4$) (Figs. 5A and B). Lipid classes were analyzed, including neutral lipids and phospholipids (Fig. 5C). As shown on the heatmap, TG levels were lower, while phosphatidylethanolamine (PE) levels were higher in WT mice with ORI treatment than those without ORI treatment (Fig. 5C). Next, detailed analysis of lipid classes with different FFA composition revealed similar results (Figs. 5D and E). ORI treatment significantly reduced TG(50:1) and TG(50:2) in the liver of HFD-fed WT mice by 56.61% and 61.03%, respectively, whereas it had no effect on LXR$\alpha^{-/-}$ mice (Fig. 5F, and Table S3). In the case of PE, the level of

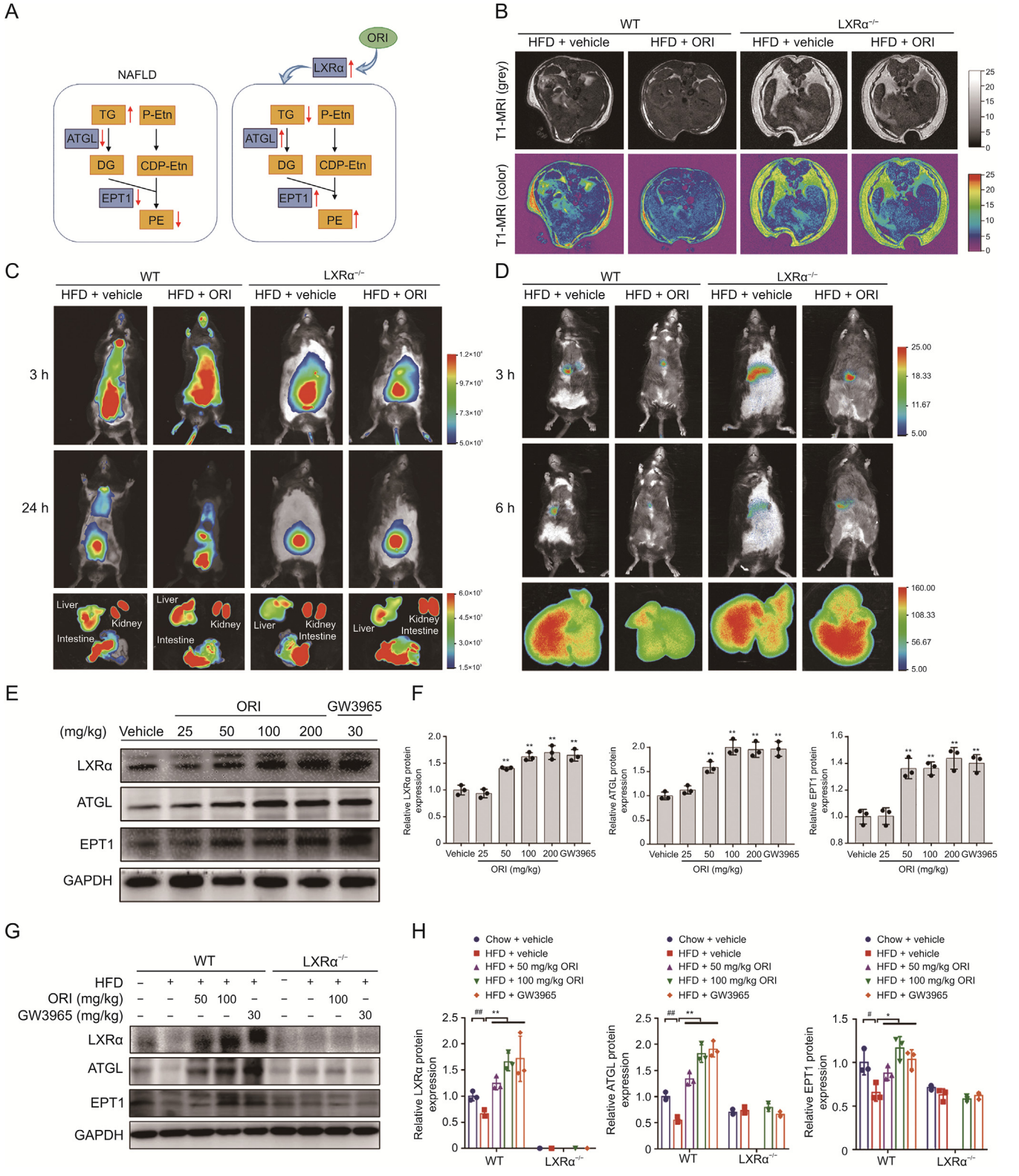

Fig. 6. Oridonin (ORI) protects against hepatic steatosis by restoring lipid homeostasis between triglyceride (TG) and phosphatidylethanolamine (PE) via the LXRα-ATGL/EPT1 pathway. (A) Schematic showing how the ORI affects lipid homeostasis. (B) Representative T1-MRI images showing lipid accumulating contents in livers of WT and LXRα$^{-/-}$ mice induced a high-fat diet (HFD) with or without ORI treatment. (C) Representative in vivo imaging system images of mice after tail vein injection of cy7-labeled phosphoethanolamine. The insert shows representative images of cy7-labeled phosphoethanolamine fluorescence intensity in mice liver, kidney and intestine. Mice livers, kidneys and intestines were collected at 24 h after tail vein injection of cy7-labeled phosphoethanolamine. (D) Representative in vivo imaging system images of mice after tail vein injection of cy7-labeled cholesterol. The insert shows representative images of cy7-labeled cholesterol fluorescence intensity in mice liver. Mice livers were collected at 6 h after tail vein injection of cy7-labeled cholesterol. (E, F) Protein expression of LXRα, ATGL and EPT1 in liver tissues of WT mice after continuously treated with various doses of ORI for 7 days ($n = 3$). Data are presented as mean ± standard deviation (SD). $^{*}P < 0.05$ and $^{**}P < 0.01$ were compared with vehicle group. (G, H) Protein expression of LXRα, and EPT1 in the livers from WT and LXRα$^{-/-}$ mice in the indicated groups. $^{\#}P < 0.05$ and $^{\#\#}P < 0.01$ were compared with Chow group; $^{*}P < 0.05$ and $^{**}P < 0.01$ were compared with HFD group. TG: triglyceride; DG: diglyceride; P-Etn: phosphoethanolamine; CDP-Etn: CDP-ethanolamine; PE: phosphatidylethanolamine.

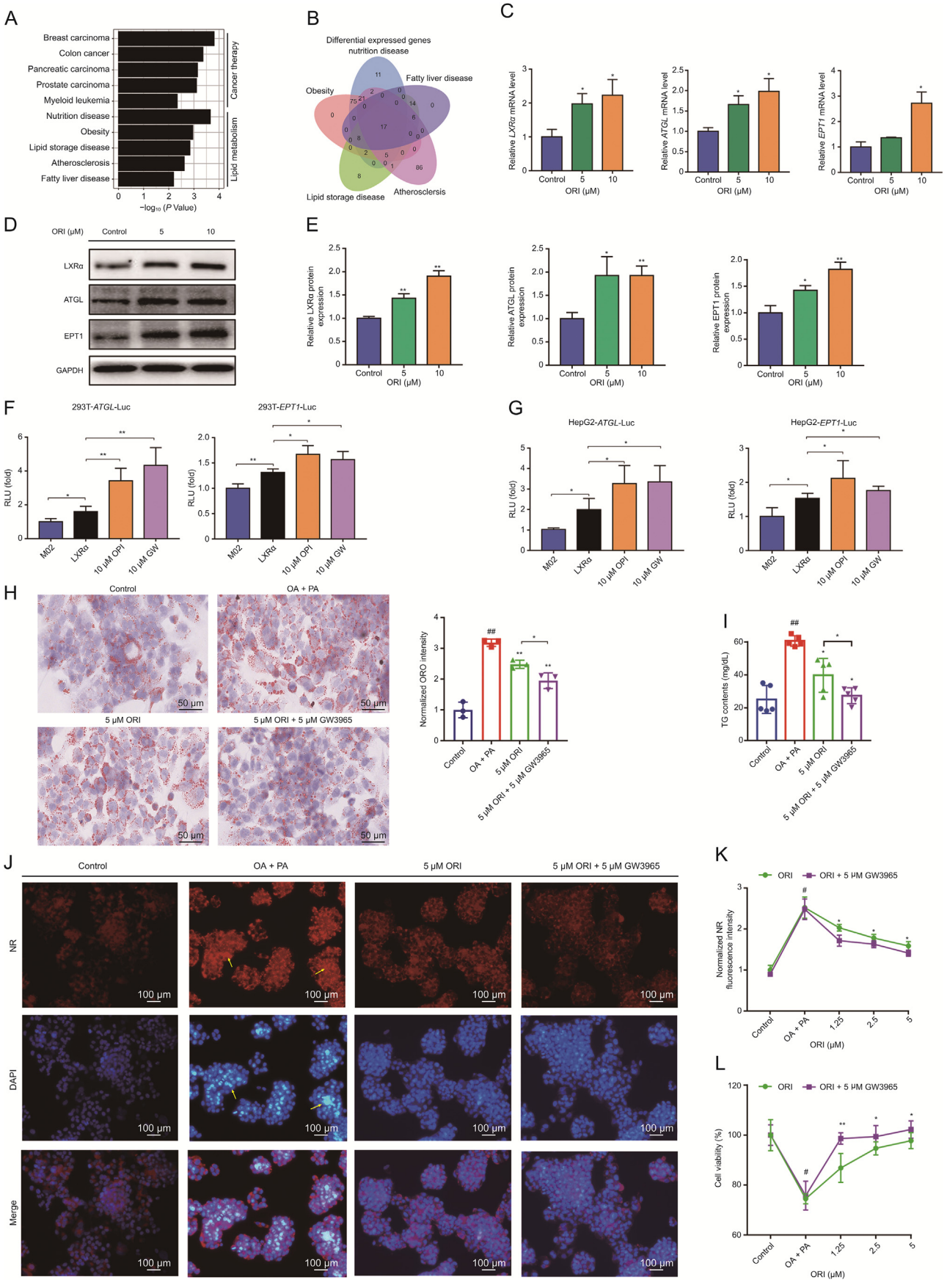
A
Breast carcinoma
Colon cancer
Pancreatic carcinoma
Prostate carcinoma
Myeloid leukemia
Nutrition disease
Obesity
Lipid storage disease
Atherosclerosis
Fatty liver disease
Cancer therapy
Lipid metabolism
−log10 (P Value)
B
Differential expressed genes nutrition disease
Obesity
Fatty liver disease
Lipid storage disease
Atherosclerosis
C
Relative LXRα mRNA level
Relative ATGL mRNA level
Relative EPT1 mRNA level
Control
5
10
ORI (μM)
D
ORI (μM)
Control
5
10
LXRα
ATGL
EPT1
GAPDH
E
Relative LXRα protein expression
Relative ATGL protein expression
Relative EPT1 protein expression
F
293T-ATGL-Luc
293T-EPT1-Luc
RLU (fold)
M02
LXRα
10 μM OPI
10 μM GW
G
HepG2-ATGL-Luc
HepG2-EPT1-Luc
H
Control
OA + PA
5 μM ORI
5 μM ORI + 5 μM GW3965
50 μm
Normalized ORO intensity
I
TG contents (mg/dL)
J
NR
DAPI
Merge
100 μm
K
ORI
ORI + 5 μM GW3965
Normalized NR fluorescence intensity
L
Cell viability (%)

PE(40:4) and PE(40:6) in WT mice treated with ORI accounted for a large proportion in PE species, which were significantly increased by 15.36% and 40.80%, respectively (Fig. 5G, and Table S4). However, the alterations of TG and PE were less remarkable in LXRα$^{-/-}$ mice with ORI treatment (Figs. 5C–G). Overall, these data clearly demonstrated that ORI restored lipid homeostasis between TG and PE through the LXRα-dependent mechanism.

3.5. ORI protects against hepatic steatosis by restoring lipid homeostasis between TG and PE via the LXRα-ATGL/EPT1 pathway

Our previous study had verified that LXRα regulates dynamic homeostasis between TG and PE via promoting *ATGL* and *EPT1* transcription and expression to alleviate hepatosteatosis [20]. Accordingly, we investigated whether ORI could ameliorate hepatic steatosis by restoring lipid homeostasis between TG and PE via the LXRα-ATGL/EPT1 pathway (Fig. 6A). As shown in the results of magnetic resonance imaging (MRI), WT mice treated with ORI displayed less hepatic lipid droplet deposition and subcutaneous fat distribution compared to those without ORI treatment (Fig. 6B). Likewise, in vivo tracking experiment with cy7-labeled phosphoethanolamine and cy7-labeled cholesterol suggested that WT mice with ORI treatment showed a higher phosphoethanolamine utilization and CHOL efflux efficiency (Figs. 6C and D). However, the ORI treatment in LXRα$^{-/-}$ mice did not affect lipid distribution, phosphoethanolamine utilization and CHOL efflux efficiency (Figs. 6B–D). An increasing fluorescence intensity was observed in liver sections from patients' histologically non-tumorous tissues (Normal), which was indicated that normal liver tissues had a higher expression of LXRα, ATGL and EPT1 than those of the nonalcoholic fatty liver (NAFL) group (Fig. S3). WT mice were orally administered with ORI (0, 25, 50, 100, 200 mg/kg) for 7 days to identify ORI as a LXRα-ATGL/EPT1 axis inducer. And the western blots showed that the protein expression of LXRα, ATGL and EPT1 were elevated by ORI or GW3965 (LXRα agonist) in the liver of WT mice (Figs. 6E and F). Moreover, ORI and GW3965 treatment upregulated the protein expression of LXRα, ATGL and EPT1 in WT mice induced by HFD feeding, but not in LXRα$^{-/-}$ mice (Figs. 6G and H). Taken together, these results indicate that ORI activates the LXRα-ATGL/EPT1 pathway, which contributes to the restoration of lipid homeostasis between TG and PE and then protects against hepatosteatosis.

3.6. ORI ameliorates the lipid accumulation and lipotoxicity in vitro by increasing the expression of ATGL and EPT1 through LXRα

HepG2 cells treated with ORI and corresponding dissolved reagent (DMSO) were evaluated by RNA-seq analysis. It is reported that ORI exerts potent anticancer activities [32–35]. Disease ontology (DO) (https://disease-ontology.org/) enrichment results are consistent with the literature, and we also revealed that ORI is related to lipid metabolism (Fig. 7A and Table S5). The differential genes in the five pathways related to lipid metabolism were analyzed by Venn diagram, and LXRα was collected and located in the overlap (Fig. 7B). Next, ORI treatment enhanced the mRNA and protein expression of LXRα, ATGL and EPT1 in HepG2 cells (Figs. 7C–E). Notably, both ORI and GW3965 could promote the induction of ATGL and EPT1 promoter activities by LXRα (Figs. 7F and G). ORI significantly reduced TG accumulation (Figs. S4A–E), and was better than atorvastatin in its ability to improve cell viability (Fig. S4F). Indeed, the combination of ORI and GW3965 (5 μM) more effectively attenuated lipid deposition and cytotoxicity (Figs. 7H–L). Altogether, these data were supported the view that ORI ameliorates lipid accumulation and lipotoxicity via activation of the LXRα-ATGL/EPT1 pathway.

3.7. ORI alleviates TG deposition and lipotoxicity in ATGL and EPT1 dependent manner, respectively

ATGL is the adipose triglyceride lipase catalyzing the initial step of TG hydrolysis [36]. EPT1 is responsible for the final step in Kennedy pathway forming PE, which is critical for phospholipid bilayers to fulfill important structural functions and a variety of cellular processes [12,13]. We hypothesized that the mechanism of ORI to alleviate lipid accumulation by regulating ATGL gene and reduce cytotoxicity through EPT1 is mutually independent. To this end, model validation of siATGL and siEPT1 on HepG2 cells was established (Fig. S5). The enhanced mRNA and protein expression of ATGL and EPT1 by ORI were significantly diminished by siLXRα treatment (Figs. 8A–C). The alleviation of TG accumulation by ORI was still observed on siEPT1 treatment but partly abolished on siATGL treatment (Fig. 8D and E). In line with this result, ORI significantly inhibited the Nile Red fluorescence intensity on siEPT1 treatment but failed to reduce the Nile Red fluorescence intensity on siATGL treatment (Figs. 8F–I). Moreover, DAPI staining and cell viability analysis exhibited that the cytoprotective effect of ORI still presented on HepG2 cells treated with siATGL but disappeared on siEPT1 treatment (Figs. 8G–J). These findings support a role of ORI in attenuating TG deposition and lipotoxicity in ATGL and EPT1 dependent manner, respectively.

4. Discussion

ORI is a major ent-kaurane diterpenoid from the traditional Chinese medicine *R. rubescens*. Inspired by its remarkable anti-steatosis activity, we performed a lipidomic profiling study and luciferase reporter assay to identify the effects and molecular mechanisms of ORI on lipid metabolism. In this paper, our results indicate that LXRα is required for the lipid-lowering and cytoprotective effects of ORI. Our previous study clarified the functions of the LXRα-ATGL/EPT1 pathway in maintaining the lipid balance between TG metabolism and PE synthesis to ameliorate hepatic steatosis and lipotoxicity [20]. Overall, ORI, as a natural activator of

Fig. 7. Oridonin (ORI) ameliorates the lipid accumulation and lipotoxicity in vitro by increasing the expression of adipose triglyceride lipase (ATGL) and ethanolamine phosphotransferase 1 (EPT1) through LXRα. (A) Disease ontology (DO) analysis of the differential genes identified by RNA-seq revealed that ORI was associated with cancer therapy and lipid metabolism(GSE112908). (B) Venn diagram showing the number of differential genes in the lipid metabolism related pathway, and LXRα was collected and located in the overlap. (C) *LXRα*, *ATGL* and *EPT1* mRNA levels in HepG2 cells treated with dimethyl sulfoxide (DMSO) or ORI ($n = 3$). Data are presented as mean ± standard deviation (SD). $^{*}P < 0.05$ was compared with DMSO group. (D, E) LXRα, ATGL and EPT1 protein levels in HepG2 cells treated with DMSO or ORI ($n = 3$). Data are presented as mean ± SD. $^{*}P < 0.05$ and $^{**}P < 0.01$ were compared with DMSO group. (F, G) LXRα induced ATGL and EPT1 transcription with ORI or GW3965 treatment in luciferase reporter assays. HepG2 cells and 293T cells were transfected with LXRα plasmid and *ATGL*-luciferase reporter or *EPT1*-luciferase reporter. After 24 h transfection, 10 μM ORI or 10 μM GW3965 was administrated and then luciferase reporter activities were measured ($n = 4$). Data are presented as mean ± SD. $^{*}P < 0.05$, $^{**}P < 0.01$. (H) Images and quantitation of ORO staining ($n = 3$). The oil red O (ORO) staining area was quantified in the insert chart. Data are presented as mean ± SD. $^{\#\#}P < 0.01$ was compared with control group; $^{*}P < 0.05$ and $^{**}P < 0.01$ were compared with oleic acid (OA) + palmitic acid (PA) group. (I) Triglyceride (TG) contents in HepG2 cells in the indicated groups simulated with OA and PA for 48 h. Data are presented as mean ± SD ($n = 5$). $^{\#\#}P < 0.01$ was compared with control group; $^{*}P < 0.05$ and $^{**}P < 0.01$ were compared with OA + PA group. (J) The neutral lipid location nile red (NR) staining and apoptotic nuclei morphology changes (DAPI staining) in HepG2 cells. Scale bar, 100 μm. (K, L) Normalized nile red (NR) fluorescence intensity (K) and cell viability (L) in HepG2 cells treated with different concentrations of ORI, which was co-treated with DMSO and GW3965. Data are mean ± SD ($n = 5$). $^{\#}P<0.05$ indicates a significant difference between control group and OA+PA group. $^{*}P < 0.05$ indicates a significant difference between the ORI group and the ORI + GW3965 group.

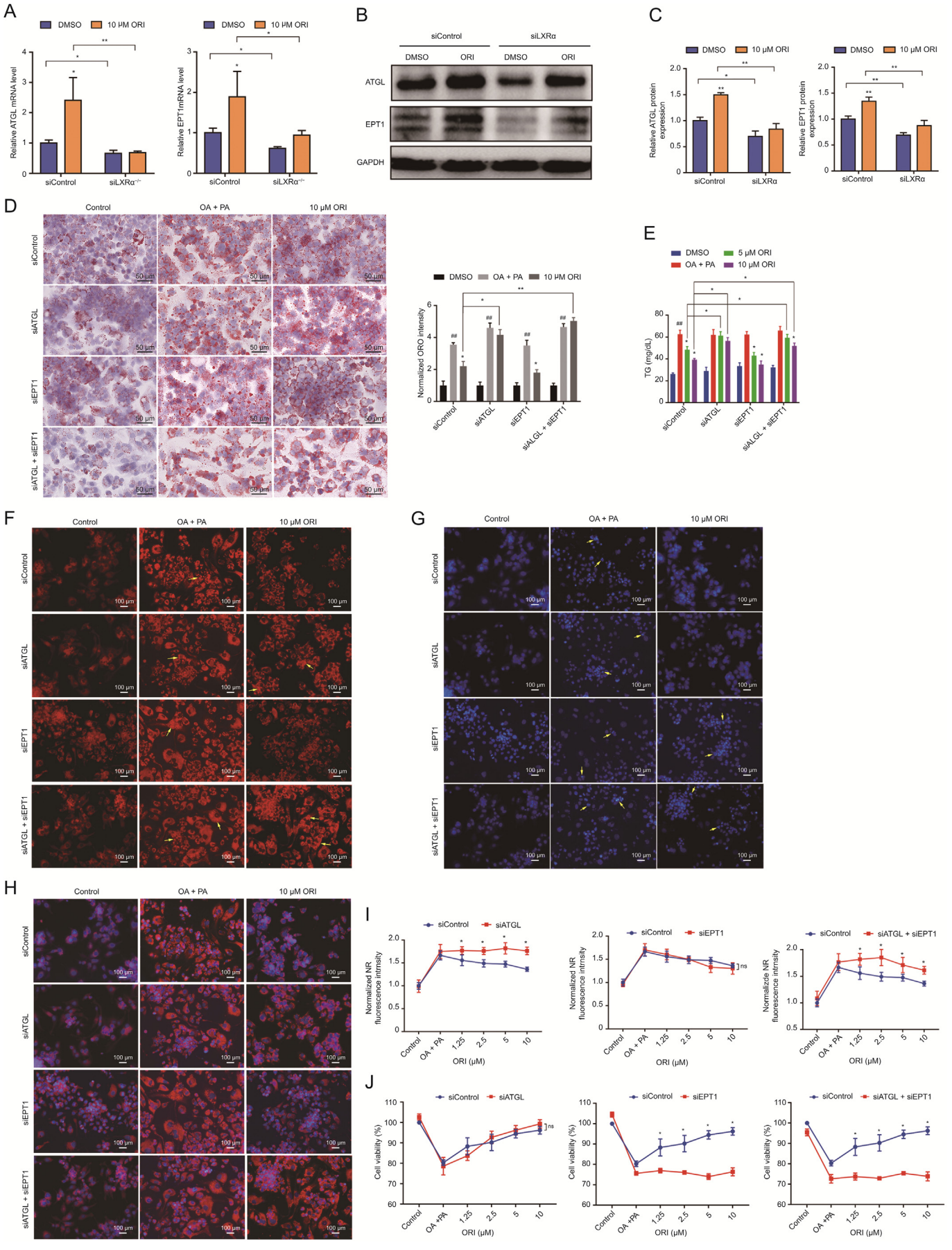
A
DMSO
10 μM ORI
Relative ATGL mRNA level
Relative EPT1mRNA level
siControl
siLXRα−/−
B
siControl
siLXRα
DMSO
ORI
ATGL
EPT1
GAPDH
C
Relative ATGL protein expression
Relative EPT1 protein expression
siControl
siLXRα
D
Control
OA + PA
10 μM ORI
siControl
siATGL
siEPT1
siATGL + siEPT1
50 μm
Normalized ORO intensity
E
5 μM ORI
TG (mg/dL)
F
100 μm
G
H
I
Normalized NR fluorescence intrnsity
ORI (μM)
J
Cell viability (%)

the LXRα-ATGL/EPT1 axis to restore lipid homeostasis between TG and PE, contributed to the improvement of hepatosteatosis and lipotoxicity.

Steatosis impairs the hepatocyte membrane integrity leading to inflammatory responses or fibrosis [7,37]. Several lines of evidence support that NAFLD and hepatic steatosis result in lipid disorder between TG and PE. It is reported that TG overload and PE reduction is one of the important lipid signatures of nonalcoholic steatohepatitis (NASH) based on the comprehensive lipidomic analysis [38]. Pcyt2 deletion produced inhibitory effects on PE synthesis, leading to elevated levels of TG [11,39]. This supports the notion that neutral lipid-lowering administration combined with phospholipid supplementation can serve as effective and safe anti-dyslipidemic therapy [21]. Promoting TG hydrolysis and phospholipid synthesis is beneficial for the recovery of nerve injury and axon regeneration [10]. Besides, dietary phospholipids might be of benefit on the treatment of fatty liver disease, which can reduce liver lipid levels [40]. To date, lipidomic research have become a valuable tool to identify and quantify all lipid components to discover the lipid alternation after treatment, which is usually involved the utilization of chromatography mass spectrometry with separation ability and high sensitivity to achieve in-depth analysis of lipids [41]. In this regard, we exploited the lipidomic profiling to demonstrate the ability of ORI treatment to diminish TG levels and increase PE levels, suggesting the potential of modulating lipid disturbances for the treatment of NAFLD.

In recent years, ORI is broadly reported to possess multiple effects like anti-inflammation and anti-tumor [24], which can alleviate cancers such as prostate carcinoma, breast cancer and colon cancer [42]. Limited researches revealed that ORI may attenuate NAFLD with strong anti-inflammasome activity through NLRP3 pathway or ROS-NF-κB [27,28]. Whereas, the exact mechanism of ORI in lipid metabolism dysfunction was not fully understood. In addition, NAFLD is an alarming public health issue worldwide, increasing the risk of insulin resistance, cardiovascular diseases, hyperlipidemia, liver diseases and even several cancers [16,43]. Statin, a commonly clinical treatment option for hyperlipidemia, is a hydroxymethyl glutaryl-CoA (HMG-CoA) reductase inhibitors, whose side effects is still associated with an increased risk of myalgia, diabetes mellitus and hepatic transaminase elevations [44–46]. Our results showed that Atorvastatin treatment had no effect on hepatic fibrosis and inflammatory factors (IL-1β and TNF-α) compared to the ORI treatment (Fig. 1G and H, J and K). And Atorvastatin is less effective than ORI at improving cell viability (Fig. S4). Our work confirmed the discovery of ORI as a natural activator for the restoration of lipid homeostasis and justifies the rationale of activating LXRα-ATGL/EPT1 pathway as an effective approach to prevent both hepatic steatosis and lipotoxicity. In view of hepatocyte protection like anti-inflammatory and antifibrotic effects, we believe that ORI may serve as an ideal candidate drug to prevent and treat associated metabolic lipid disorders (Figs. 1 and 2).

LXRα is now recognized to be fundamental in controlling energy balance and lipid homeostasis [18], such as CHOL excretion [47], glucose metabolism and phospholipid remodeling [18]. In our previous study, WT mice were orally administered with ORI (0, 25, 50, 100, 200 mg/kg) for 7 days to clarify ORI toxicity. The results showed that both the body weight and liver function did not differ between the control and ORI treatment groups in WT mice, indicating that ORI had no obvious toxicity within 200 mg/kg. A similar study also reported that ORI had no obvious toxicity within 200 mg/kg and markedly induced hepatic metabolizing enzyme activity at doses of 50–100 mg/kg [48]. Out of these investigations, we selected 50 mg/kg and 100 mg/kg for scientific research on C57 mice. Our results showed that the beneficial effects of ORI on NAFLD were absent in LXRα$^{-/-}$ mice, suggesting that the anti-steatosis activity of ORI depends on LXRα activation (Figs. 3 and 4). In our previous work, direct regulation of ATGL and EPT1 by LXRα was validated [20]. This study not only identified the protective effect of ORI against NAFLD by maintaining lipid balance (Fig. 5), but also uncovered an intrinsic mechanism by which ORI regulates both the ATGL gene associated with TG metabolism and the EPT1 gene involved in PE biosynthesis via LXRα signaling (Figs. 6 and 7). Therefore, ORI lost its effect on decreasing TG accumulation in siATGL treatment. In parallel with this result, siEPT1 treatment suppressed the improvement of ORI on lipotoxicity (Fig. 8).

5. Conclusions

In conclusion, our study supports the therapeutic value of ORI in NAFLD treatment, which not only reduces hepatic fat overload, but also exerts a hepatocyte protective effect to reduce inflammation and fibrosis. Indeed, we may provide the first evidence that the activation of the LXRα-ATGL/EPT1 pathway by ORI contributes to the restoration of lipid homeostasis between TG and PE, thereby ameliorating hepatosteatosis and lipotoxicity.

CRediT author statement

Yulian Chen: Methodology, Investigation, Formal analysis, Visualization, Writing - Original draft preparation; **Huanguo Jiang** and **Zhikun Zhan**: Methodology, Validation, Formal analysis, Writing - Original draft preparation; **Jindi Lu**, **Tanwei Gu**, **Ping Yu**, **Weimin Liang** and **Xi Zhang**: Investigation, Writing - Reviewing and Editing; **Shilong Zhong**: Resources, investigation; **Lan Tang**: Conceptualization, Resources, Project administration, Writing - Reviewing and Editing.

Declaration of competing interest

The authors declare that there are no conflicts of interest.

Acknowledgments

This work was supported by the National Natural Science Foundation of China (Grant No.: 81973388), Marine Economy Development Project of Guangdong Province (Project No.: GDNRC [2021]52), and the Key Research and Development Program of Guangdong Province (Program No.: 2020B1111030005).

Fig. 8. Oridonin (ORI) alleviates triglyceride (TG) deposition and lipotoxicity in ATGL and EPT1 dependent manner, respectively. (A–C) ATGL and EPT1 mRNA ($n = 3$) and protein ($n = 3$) levels in HepG2 cells treated with 10 μM ORI for 48 h after transfection with siLXRα or siControl. Data are mean ± standard deviation (SD). $^{*}P < 0.05$, $^{**}P < 0.01$. (D) Oil red O (ORO) staining of HepG2 cells treated with 10 μM ORI for 48 h in response to oleic acid (OA) and palmitic acid (PA) after transfection with siATGL, siEPT1 or siControl. Scale bar, 50 μm. The ORO staining area was quantified in the insert chart. Data are mean ± SD ($n = 3$). $^{\#}P < 0.05$ and $^{\#\#}P < 0.01$ were compared with dimethyl sulfoxide (DMSO) group. $^{*}P < 0.05$ and $^{**}P < 0.01$ were compared with OA + PA group. (E) TG contents in HepG2 cells treated with ORI after transfection with siATGL, siEPT1 or siControl in response to OA and PA. Data are mean ± SD ($n = 5$). $^{\#}P < 0.05$ and $^{\#\#}P < 0.01$ were compared with DMSO group. $^{*}P < 0.05$ and $^{**}P < 0.01$ were compared with OA + PA group. (F–H) The neutral lipid location (NR staining) (F) and apoptotic nuclei morphology changes (DAPI) (G), and their merged images (H) in HepG2 cells treated with 10 μM ORI after transfection with siATGL, siEPT1 or siControl in response to OA and PA ($n = 3$). (I, J) Normalized Nile red (NR) fluorescence intensity and cell viability in HepG2 cells treated with different concentrations of ORI after transfection with siATGL, siEPT1 or siControl in response to OA and PA. The higher the fluorescence intensity value, the higher the lipid accumulation level in the cell. Data are mean ± SD ($n = 5$). $^{*}P < 0.05$ indicates a significant difference between the siControl group and the siATGL, siEPT1 or siATGL + siEPT1 group.

Appendix A. Supplementary data

Supplementary data to this article can be found online at https://doi.org/10.1016/j.jpha.2023.08.010.

References

[1] B. Swinburn, G. Sacks, E. Ravussin, Increased food energy supply is more than sufficient to explain the US epidemic of obesity, Am. J. Clin. Nutr. 90 (2009) 1453–1456.
[2] F. Seebacher, A. Zeigerer, N. Kory, et al., Hepatic lipid droplet homeostasis and fatty liver disease, Semin. Cell Dev. Biol. 108 (2020) 72–81.
[3] A. Cano, C. Alonso, Deciphering non-alcoholic fatty liver disease through metabolomics, Biochem. Soc. Trans. 42 (2014) 1447–1452.
[4] V. Manne, P. Handa, K.V. Kowdley, Pathophysiology of Nonalcoholic Fatty Liver Disease/Nonalcoholic Steatohepatitis, Clin. Liver Dis. 22 (2018) 23–37.
[5] G.A. Michelotti, M.V. Machado, A.M. Diehl, NAFLD, NASH and liver cancer, Nat Rev Gastroenterol. Hepatol. 10 (2013) 656–665.
[6] M. Trauner, M. Arrese, M. Wagner, Fatty liver and lipotoxicity, Biochim. Biophys. Acta 1801 (2010) 299–310.
[7] M.E. Ertunc, G.S. Hotamisligil, Lipid signaling and lipotoxicity in metaflammation: indications for metabolic disease pathogenesis and treatment, J. Lipid Res. 57 (2016) 2099–2114.
[8] T. Li, W. Guo, Z. Zhou, Adipose Triglyceride Lipase in Hepatic Physiology and Pathophysiology, Biomolecules 12 (2021), 57.
[9] R. Schreiber, H. Xie, M. Schweiger, Of mice and men: The physiological role of adipose triglyceride lipase (ATGL), Biochim. Biophys. Acta Mol. Cell Biol. Lipids 1864 (2019) 880–899.
[10] C. Yang, X. Wang, J. Wang, et al., Rewiring Neuronal Glycerolipid Metabolism Determines the Extent of Axon Regeneration, Neuron. 105 (2020) 276–292.e275.
[11] A. Selathurai, G.M. Kowalski, M.L. Burch, et al., The CDP-Ethanolamine Pathway Regulates Skeletal Muscle Diacylglycerol Content and Mitochondrial Biogenesis without Altering Insulin Sensitivity, Cell Metab. 21 (2015) 718–730.
[12] Y. Horibata, O. Elpeleg, A. Eran, et al., EPT1 (selenoprotein I) is critical for the neural development and maintenance of plasmalogen in humans, J. Lipid Res. 59 (2018) 1015–1026.
[13] C. Ma, V. Martinez-Rodriguez, P.R. Hoffmann, Roles for Selenoprotein I and Ethanolamine Phospholipid Synthesis in T Cell Activation, Int. J. Mol. Sci. 22 (2021), 11174.
[14] J.N. van der Veen, J.P. Kennelly, S. Wan, et al., The critical role of phosphatidylcholine and phosphatidylethanolamine metabolism in health and disease, Biochim. Biophys. Acta Biomembr. 1859 (9 Pt B) (2017) 1558–1572.
[15] M.Y. Ahmed, A. Al-Khayat, F. Al-Murshedi, et al., A mutation of EPT1 (SELENOI) underlies a new disorder of Kennedy pathway phospholipid biosynthesis, Brain 140 (2017) 547–554.
[16] H. Yoon, J.L. Shaw, M.C. Haigis, et al., Lipid metabolism in sickness and in health: Emerging regulators of lipotoxicity, Mol. Cell 81 (2021) 3708–3730.
[17] P.A. Edwards, M.A. Kennedy, P.A. Mak, LXRs; oxysterol-activated nuclear receptors that regulate genes controlling lipid homeostasis, Vascul. Pharmacol. 38 (2002) 249–256.
[18] B. Wang, P. Tontonoz, Liver X receptors in lipid signalling and membrane homeostasis, Nat. Rev. Endocrinol. 14 (2018) 452–463.
[19] C. Hong, P. Tontonoz, Coordination of inflammation and metabolism by PPAR and LXR nuclear receptors, Curr. Opin. Genet. Dev. 18 (2008) 461–467.
[20] Y. Chen, H. Jiang, Z. Zhan, et al., Restoration of lipid homeostasis between TG and PE by the LXRα-ATGL/EPT1 axis ameliorates hepatosteatosis, Cell Death Dis. 14 (2023), 85.
[21] A. Sahebkar, Fat lowers fat: purified phospholipids as emerging therapies for dyslipidemia, Biochim. Biophys. Acta 1831 (2013) 887–893.
[22] S. Kadota, P. Basnet, E. Ishii, et al., Antibacterial activity of trichorabdal A from Rabdosia trichocarpa against Helicobacter pylori, Zentralbl. Bakteriol. 286 (1997) 63–67.
[23] Y. Ding, C. Ding, N. Ye, et al., Discovery and development of natural product oridonin-inspired anticancer agents, Eur. J. Med. Chem. 122 (2016) 102–117.
[24] X. Li, C.T. Zhang, W. Ma, et al., Oridonin: A Review of Its Pharmacology, Pharmacokinetics and Toxicity, Front. Pharmacol. 12 (2021), 645824.
[25] Z. Ma, C. Hu, Y. Zhang, Therapeutic effect of Rabdosia rubescens aqueous extract on chronic pharyngitis and its safety, Zhong Nan Da Xue Xue Bao Yi Xue Ban 36 (2011) 170–173.
[26] S. Chen, J. Liu, H. Zhang, Efficacy of rabdosia rubescens in the treatment of gingivitis, J. Huazhong Univ. Sci. Technolog. Med. Sci. 29 (2009) 659–663.
[27] H. He, H. Jiang, Y. Chen, et al., Oridonin is a covalent NLRP3 inhibitor with strong anti-inflammasome activity, Nat. Commun. 9 (2018) 2550.
[28] Y. Zhu, S. Ruan, H. Shen, et al., Oridonin regulates the polarized state of Kupffer cells to alleviate nonalcoholic fatty liver disease through ROS-NF-κB, Int. Immunopharmacol. 101 (2021), 108290.
[29] T. Zhang, Y. Chen, Z. Zhan, et al., Oridonin alleviates d-GalN/LPS-induced acute liver injury by inhibiting NLRP3 inflammasome, Drug Dev. Res. 82 (2021) 575–580.
[30] T.T. Sham, C.O. Chan, Y.H. Wang, et al., A review on the traditional Chinese medicinal herbs and formulae with hypolipidemic effect, Biomed. Res. Int. 2014 (2014), 925302.
[31] Z. Zhan, F. Dai, T. Zhang, et al., Oridonin alleviates hyperbilirubinemia through activating LXRα-UGT1A1 axis, Pharmacol. Res. 178 (2022), 106188.
[32] Z. Yao, F. Xie, M. Li, et al., Oridonin induces autophagy via inhibition of glucose metabolism in p53-mutated colorectal cancer cells, Cell Death Dis. 8 (2017), e2633.
[33] Z. Gui, F. Luo, Y. Yang, et al., Oridonin inhibition and miR-200b-3p/ZEB1 axis in human pancreatic cancer, Int. J. Oncol. 50 (2017) 111–120.
[34] X. Li, X. Li, J. Wang, et al., Oridonin up-regulates expression of P21 and induces autophagy and apoptosis in human prostate cancer cells, Int. J. Biol. Sci. 8 (2012) 901–912.
[35] G.B. Zhou, H. Kang, L. Wang, et al., Oridonin, a diterpenoid extracted from medicinal herbs, targets AML1-ETO fusion protein and shows potent antitumor activity with low adverse effects on t(8;21) leukemia in vitro and *in vivo*, Blood 109 (2007) 3441–3450.
[36] K. Brejchova, F.P.W. Radner, Distinct roles of adipose triglyceride lipase and hormone-sensitive lipase in the catabolism of triacylglycerol estolides, Proc. Natl. Acad. Sci. U S A. 118 (2021), e2020999118.
[37] C.L. Chen, Y.C. Lin, Autophagy Dysregulation in Metabolic Associated Fatty Liver Disease: A New Therapeutic Target, Int. J. Mol. Sci. 23 (2022), 10055.
[38] F. Chiappini, A. Coilly, H. Kadar, et al., Metabolism dysregulation induces a specific lipid signature of nonalcoholic steatohepatitis in patients, Sci. Rep. 7 (2017), 46658.
[39] E. Calzada, O. Onguka, S.M. Claypool, Phosphatidylethanolamine Metabolism in Health and Disease, Int. Rev. Cell Mol. Biol. 321 (2016) 29–88.
[40] J.S. Cohn, E. Wat, A. Kamili, et al., Dietary phospholipids, hepatic lipid metabolism and cardiovascular disease, Curr. Opin. Lipidol. 19 (2008) 257–262.
[41] T. Xu, C. Hu, Q. Xuan, et al., Recent advances in analytical strategies for mass spectrometry-based lipidomics, Anal. Chim. Acta. 1137 (2020) 156–169.
[42] Z. Liu, L. Ouyang, H. Peng, et al., Oridonin: targeting programmed cell death pathways as an anti-tumour agent, Cell Prolif. 45 (2012) 499–507.
[43] R.C. Huang, L.J. Beilin, O. Ayonrinde, et al., Importance of cardiometabolic risk factors in the association between nonalcoholic fatty liver disease and arterial stiffness in adolescents, Hepatology 58 (2013) 1306–1314.
[44] M. Ruscica, N. Ferri, M. Banach, et al., Side effects of statins-from pathophysiology and epidemiology to diagnostic and therapeutic implications, Cardiovasc. Res. 118 (2023) 3288–3304.
[45] S.M. Grundy, J.I. Cleeman, C.N. Merz, et al., Implications of recent clinical trials for the National Cholesterol Education Program Adult Treatment Panel III guidelines, Circulation 110 (2004) 227–239.
[46] R. Balasubramanian, N.M.P. Maideen, HMG-CoA Reductase Inhibitors (Statins) and their Drug Interactions Involving CYP Enzymes, P-glycoprotein and OATP Transporters-An Overview, Curr. Drug Metab. 22 (2021) 328–341.
[47] S.U. Naik, X. Wang, J.S. Da Silva, et al., Pharmacological activation of liver X receptors promotes reverse cholesterol transport in vivo, Circulation 113 (2006) 90–97.
[48] Y.W. Zhang, M.H. Bao, L. Hu, et al., Dose-response of oridonin on hepatic cytochromes P450 mRNA expression and activities in mice, J Ethnopharmacol 155 (2014) 714–720.